

Estimates of PM_{2.5} concentrations spatiotemporal evolution across China considering aerosol components in the context of the Reform and Opening-up

Su Ding ^{a,b,c,*}, Zhiwei Wei ^{d,e}, Jianhua He ^{f,g}, Dianfeng Liu ^{f,g}, Rong Zhao ^h

^a State Key Laboratory of Subtropical Silviculture, Zhejiang A & F University, Hangzhou, 311300, China

^b Key Laboratory of Carbon Cycling in Forest Ecosystems and Carbon Sequestration of Zhejiang Province, Zhejiang A & F University, Hangzhou, 311300, China

^c School of Environmental and Resources Science, Zhejiang A & F University, Hangzhou 311300, China

^d School of Remote Sensing & Geomatics Engineering, Nanjing University of Information Science and Technology, Nanjing, 210044, China

^e Key Laboratory of Network Information System Technology (NIST), Aerospace Information Research Institute, Chinese Academy of Sciences, Beijing, 100190, China

^f School of Resource and Environmental Sciences, Wuhan University, Wuhan, 430079, China

^g Key Laboratory of Geographic Information System, Ministry of Education, Wuhan University, Wuhan, 430079, China

^h Vanke School of Public Health, Tsinghua University, Beijing 100084, China

ARTICLE INFO

Keywords:

PM_{2.5} concentration

MERRA-2

Long-term trend

Aerosol components

ABSTRACT

With astonishing and rapid development in China since the Reform and Opening-up in 1978, serious air pollution has become a great challenge. A better understanding of the response of PM_{2.5} pollution to socioeconomic development after the Reform and Opening-up policy is benefit for pollution control. However, heterogeneous influences of biophysical and socioeconomic activities on PM_{2.5} pollution pose great challenges in statistical simulation of PM_{2.5}. Few statistical model regards aerosol species as the explanatory variables for heterogeneous formation mechanism to retrieve PM_{2.5} concentration. In this research, monthly PM_{2.5} concentration in China during 1980–2020 was reconstructed by a novel statistical strategy considering aerosol components (AC-RF). Three cross-validation (CV) methods, sample-based CV, spatial-based CV and temporal-based CV results indicated satisfactory performance of AC-RF model with correlation coefficient (R) of 0.92, 0.90, 0.86, respectively. A three-stage concluded on PM_{2.5} concentration annual variation in China was drawn as followed: Before 2000, PM_{2.5} level in China represented smooth evolution and mainly influenced by natural events with polluted region locating in Xinjiang province, North China and Central China. Since 2000, PM_{2.5} concentration increased to high level in the context of rapid socioeconomic development. Severe air pollution covered Jing-Jin-Ji agglomeration, Central China and Sichuan Basin. During 2012–2020, PM_{2.5} declined and polluted region shrank, which was benefited by the strictest-ever air pollution control measures. Based on aerosol components analysis, sulfate aerosol exhibited the most significant increase trend in recent 40 years and black aerosol variation is the most closely related to PM_{2.5} pollution. In conclusion, unsustainable development is the culprit for air quality deterioration. Strict and continuous air pollution control strategies are effective for air quality improvement.

1. Introduction

Since the implementation of the Reform and Opening-up in 1978, industrialization and urbanization in China has experienced astonishing and rapid development. However, flourishing economy is at the expense of environment destruction. A myriad of pollutants from anthropogenic activities have been emitted into atmosphere and PM_{2.5} was served as one of the main air pollutants. PM_{2.5} refers to the particulate matter

which is less than 2.5 μm in aerodynamic equivalent diameter with multi components. Huge threaten to human health is caused for its small size and toxicity (Lelieveld et al., 2015). There are about 3.2 million premature deaths due to high PM_{2.5} exposure every year in terms of relative study (Lim et al., 2013). Moreover, soil acidification given rise by sulfate and nitrate aerosols deposition that the main components of PM_{2.5} as well as solar radiation reduction caused by PM_{2.5} pollution decrease crop yields by 5%–30% (Chameides et al., 1999). In recent years,

* Corresponding author.

E-mail address: suding@whu.edu.cn (S. Ding).

deteriorating air quality in China has led to large economic loss. In Beijing, the economic loss caused by air pollution is of nearly 1 million dollars during 2013, which accounts for 0.08% of total GDP (Gao et al., 2015). Consequently, investigation of PM_{2.5} evolution in the context of the Reform and Opening-up implementation provides insights into the impacts of development path. Using effective method to estimate PM_{2.5} evolution in recent 40 years is the basis of air pollution treatment strategy formulation.

Ground monitoring and model retrieval data both can describe surface PM_{2.5} evolution effectively. Since monitoring data fail to represent the space continuity distribution of PM_{2.5} and lack the data preceding 2013. Model retrieval based on the factors reflecting atmospheric turbidity has been applied widely in long-term and full-coverage PM_{2.5} pollution mapping. MODIS AOD are one of the most popular datasets for PM_{2.5} retrieval in recent research (Li et al., 2007; van Donkelaar et al., 2010; Hu et al., 2014). Nevertheless, MODIS AOD dataset only monitor the atmospheric turbidity after 2002 (Jiang et al., 2021; Wei et al., 2021). There is previous research reconstructing PM_{2.5} concentration before 2002 by using visibility observation data (Li et al., 2021; Liu et al., 2017). Other scientific publications calculate the ratio of PM_{2.5} concentration and aerosol extinction coefficient to simulate PM_{2.5} based on visibility data by using GEOS-Chem chemical transport model (Li et al., 2020). Whereas, spatial continuity dataset is obtained by interpolating the simulations of individual sites. Interpolation methods only consider spatial interrelation and there is still uncertainty.

Compared with MODIS AOD and visibility, MERRA-2 AOD dataset is characterized as excellent spatiotemporal completeness. MERRA-2 AOD datasets can describe atmospheric turbidity during the period from 1980 to the present. Based on previous scientific publications, MERRA-2 AOD is in good agreement with AOD observation around the world based on the verification with CARSNET (Aerosol Robotic Network) monitoring data (Randles et al., 2017; Che et al., 2019). It also have been documented that MERRA-2 AOD dataset can monitor the atmospheric turbidity degree in China (Song et al., 2018; Sun et al., 2019). Apart from AOD dataset, MERRA-2 aerosol diagnostics datasets also involve aerosol components surface mass concentration and AOD (Randles et al., 2017; Song et al., 2018; Ding et al., 2020). It has been introduced to conduct the investigations about the evolution of aerosol composition around the world (Rawat et al., 2019; Rizza et al., 2019). Moreover, PM_{2.5} concentration is estimated directly by using MERRA-2 aerosol components data in previous research (Ma et al., 2020; Provencal et al., 2017). However, it has been verified that this method significantly underestimates PM_{2.5} pollution compared with monitoring data since nitrate aerosol is excluded. Nitrate aerosol is an indispensable component in haze cases. Especially in North China, it accounts for more than 20% of PM_{2.5} concentration during winter (Song et al., 2018). As a consequence, it requires employing the model describing the relationship between PM_{2.5} and MERRA-2 dataset variables for PM_{2.5} concentration retrieval.

It is worth noting that PM_{2.5} spatiotemporal pattern is of significant heterogeneity causing by meteorology condition variation and unbalance pollutant emission. On the one hand, PM_{2.5} diffusion and secondary PM_{2.5} formation are related with meteorology condition closely (Liu et al., 2020; Zheng et al., 2015). On the other hand, underlying surface complexity and anthropogenic emission sources variety both cause the difference of air pollutant emission across China (Zheng et al., 2018). Aerosol components in PM_{2.5} is the embodiment for spatiotemporal characteristics of pollutants emission as well as one of the causes for PM_{2.5} spatiotemporal evolution, since impacts of atmospheric factors on PM_{2.5} concentration vary from aerosol species (Tai et al., 2010). Consequently, aerosol components can be regarded as effective factors for explaining the spatiotemporal heterogeneity of PM_{2.5} pollution. Nevertheless, previous PM_{2.5} modeling introduces geographical and temporal weights to estimate PM_{2.5} formation heterogeneity (He and Huang, 2018a, 2018b). There are few studies employing aerosol species to explore the heterogeneity of PM_{2.5} pollution.

Considering the lack of aerosol components regarded as the explanatory variables for PM_{2.5} formation heterogeneity in statistical model, we introduced a random forest model integrating AOD, aerosol components AOD and meteorology variables to presented a complete picture of PM_{2.5} spatiotemporal evolution during 1980–2020 in this research. Based on the MERRA-2 aerosol components surface mass concentration, aerosol compositions spatiotemporal patterns in China were also investigated during recent 40 years.

2. Data and method

2.1. Study area

In this research, China with diverse geographical characters was regarded as study area in this research. Due to vast territory, China is of complicated climate types and humidity varies across China. Thus, underlying surface environment is characterized as heterogeneity. Abundant precipitation and fertile soil result in about 92% of cropland and forest distributing in eastern China. Furthermore, the urban agglomerations with dense population and active socioeconomic activities including Jing-Jin-Ji, Yangtze River Delta and Pearl River Delta also distribute in eastern China. In northwestern China, the land type mainly consists of desert, gobi and saline-alkali land caused by the scarcity of precipitation. Comprehensively considering environment and socio-economic status, China territory was divided into seven regions in this study (Fig. 1).

2.2. Data source and processing

Datasets including surface monitoring PM_{2.5} concentration, PM_{2.5} simulation dataset, aerosol diagnostics and meteorology reanalysis data were collected from multi-source for PM_{2.5} concentration estimation in China during 1980–2020. It is described in detail as Table S1.

2.2.1. Surface PM_{2.5} monitoring and PM_{2.5} simulation data

PM_{2.5} monitoring concentration is obtained from China National Environmental Monitoring Centre (CNEMC) platforms (1640 stations), US consulates stations in China, Taiwan and Hong Kong local environmental protection agencies (88 stations). The distribution of air

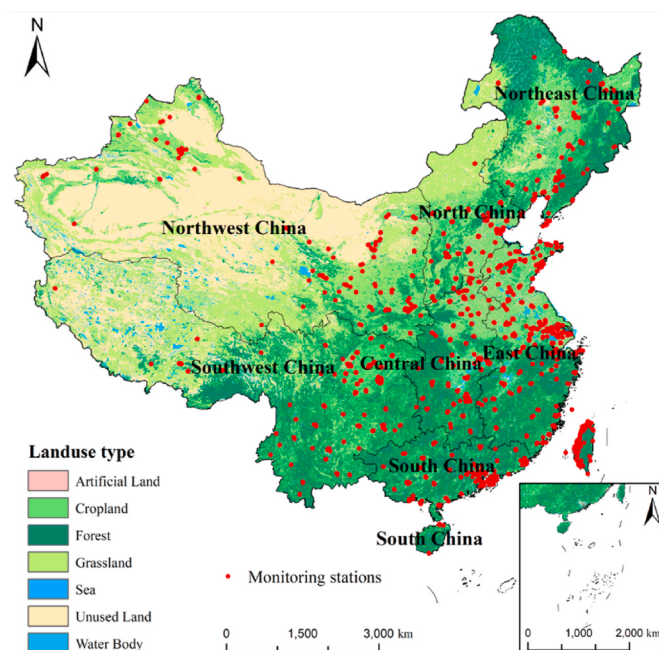


Fig. 1. Study area and the distribution of air pollutants monitoring stations.

pollutants monitoring stations is showed as Fig. 1. Both hourly and monthly in-situ observations of PM_{2.5} data during May 1997 to December 2020 are originated from these 1728 air pollutants monitoring stations across China. The PM_{2.5} measured by CNEMC was serviced as training dataset for AC-RF model and others was applied in external verification. Besides, missing data removal and average calculation were completed before the data integration. Monthly PM_{2.5} concentration is the arithmetic average value of raw hourly data. In this research, PM_{2.5} simulation dataset collected from research achievement of Atmospheric Composition Analysis Group was also integrated into training dataset (Hammer et al., 2020). Compared with in-situ PM_{2.5} measurements, this dataset was in good accordance with PM_{2.5} monitor concentration with an out-of-sample cross-validated (CV) R value of 0.90 at global scale and R value of 0.75 in China (Bai et al., 2019; Hammer et al., 2020).

2.2.2. MERRA-2 assimilated aerosol diagnostics dataset

MERRA-2 aerosol dataset is assimilated and retrieved based on the AOD from MODIS, Advanced Very High Resolution Radiometer instruments (AVHRR), Multiangle Imaging Spectro Radiometer (MISR) and Aerosol Robotic Network (AERONET) sunphotometer stations (Buchard et al., 2017; Song et al., 2018). This dataset consists of AOD, aerosol component AOD and aerosol component surface mass concentration (Global Modeling and Assimilation Office, 2015). Compared with AERONET observation during 2003–2017, MERRA-2 AOD had a small deviation with overall MBE of −0.009 and RMSE of 0.126 at global scale (Gueymard and Yang, 2020). In China, MERRA-2 AOD also achieved a good agreement with AERONET AOD data and correlation coefficients during four seasons were larger than 0.87. However, MERRA-2 AOD was lower than AERONET observation all the time with mean bias error (MEB) of −0.05 and MERRA-2 AOD in winter had the largest bias (Che et al., 2019; Sun et al., 2019). Since the exclusion of nitrate aerosol from MERRA-2 dataset results in slightly underestimates of AOD. Besides, the aerosol model used by MERRA-2 reanalysis dataset is lack of pollutant emission data (Buchard et al., 2017).

Aerosol components dataset was derived from GOCART model. It also has been verified with ground monitor observations and can capture the atmospheric pollutant components characteristics. Hung et al. (2019) indicated that MERRA-2 aerosol components dataset represents strong consistent trend with in-situ observations in Taiwan. Xu et al. (2020) found that MERRA-2 aerosol was competent for delivering the spatiotemporal characteristic of black carbon (BC) aerosol in East China. The column mass of dust aerosol in atmospheric above Sahara Desert also could be simulated accurately by MERRA-2 datasets (Kishcha et al., 2015). Although there is uncertainty in MERRA-2 aerosol diagnostics dataset, AOD spatiotemporal characteristic can still be capture by MERRA-2 reanalysis dataset.

2.2.3. Meteorology reanalysis dataset

PM_{2.5} formation and diffusion are influenced by meteorology conditions (Chen et al., 2018; Ding et al., 2020). Thus, meteorology factors were also served as additional covariates to improve simulation precision. In this research, there are eight meteorology variables collected from ERA5 reanalysis data with the spatial resolution of 0.25° × 0.25° (Hersbach et al., 2020). ERA5 is the fifth generation European Centre for Medium Range Weather Forecasts (ECMWF) reanalysis for the global climate and weather from 1950 onwards. This reanalysis data combine the model data with observations by assimilation method. Both MERRA-2 aerosol diagnostics and meteorology reanalysis dataset were of raster format and clipped based on China land territory.

2.3. PM_{2.5} retrieval and spatiotemporal analysis

2.3.1. AC-RF construction and PM_{2.5} retrieval

The processes of PM_{2.5} retrieval and spatiotemporal analysis are showed in Fig. 2. On the basis of spatial grid with resolution of 0.25° ×

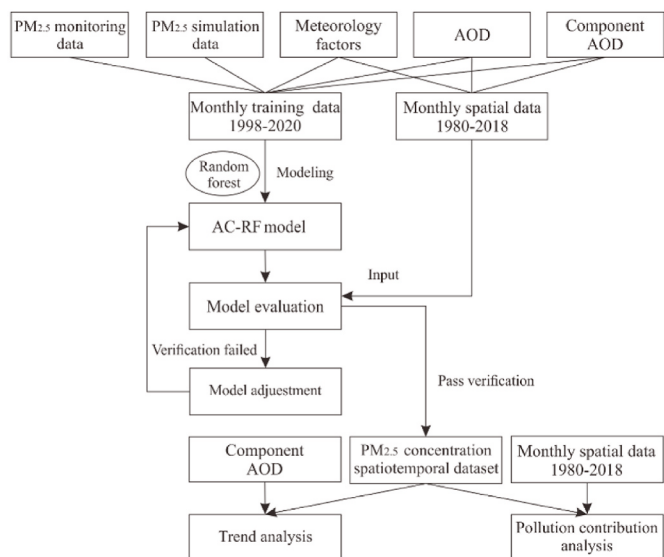


Fig. 2. Schematic of PM_{2.5} retrieval and spatiotemporal characteristics analysis.

0.25°, these five datasets were matched spatially and temporally within China. As for PM_{2.5} monitoring data, average calculation was applied when one grid cell contains more than one monitoring site. PM_{2.5} simulation data during 1998–2014 and surface monitor data during the period from 2015 to 2020 were both served as training data for AC-RF model construction. PM_{2.5} concentration during 1980–2020 were estimated by inputting predictors spatiotemporal datasets into AC-RF model. Subsequently, the spatiotemporal evolution analysis based on Theil-Sen Median and Mann-Kendall methods for both PM_{2.5} and aerosol species concentration were carried out. At last, spatial correlation between PM_{2.5} concentration and influence factors were estimated.

2.3.2. AC-RF construction and verification

RF is one of ensemble machine learning algorithms, whose outcomes synthesize the simulations of several basic classifier (Breiman, 2001). Class and Regression Tree (CART) is the basic classifier of random forest. When construct random forest, boot-strap is applied in random forest. The set D containing K samples is selected randomly with put back from the training dataset to build k trees. The portion is not drawn called out of bag (OOB), which is used to verify model performance. In this research, there were 130,237 samples and 14 independent variables in training dataset. In the node of each tree, a variable is selected from m ($m < 14$) variables to grow based on the principle of minimum variances. Each feature j in subset D_i ($i = 1, 2, \dots, k$) is traversed and input space is divided into several regions according to all of the value of feature j . If the value of feature j is s , the input space is divided into two regions as follows:

$$R_1(j, s) = \{x | x^{(j)} \leq s\} \quad R_2(j, s) = \{x | x^{(j)} > s\} \quad (1)$$

Loss function is also calculated and segmentation point is the minimum value of loss function.

$$\min \left[\sum_{x_i \in R_1(j, s)} (y_i - c_1)^2 + \sum_{x_i \in R_2(j, s)} (y_i - c_2)^2 \right] \quad (2)$$

where c_1 and c_2 are the average outcomes of interval R_1 and R_2 , respectively. These two split subsets are also divided in the same way. Finally, there are l intervals R_1, R_2, \dots, R_l and CART can be expressed as follows:

$$f(x) = \sum_{l=1}^L c_l I(x \in R_l) \quad (3)$$

where c_l is the average value of $\text{PM}_{2.5}$ concentration simulation of i th region. The comprehensive simulation of all CART is output as RF model outcome.

Subsequently, three tenfold cross-validation (CV) methods named sample-based CA, spatial-based CV and temporal-based CV were employed to examine model accuracy. Training data was divided into ten parts evenly and extracted nine groups to fit model. The rest one group data was served to validate model performance. This process was repeated iteratively until all the data had been modeled and validated. Particularly, as for spatial-based CV and temporal-based CV, division of training and verification set is based on spatial grids code and year, respectively. Part of data from some sites or one year is removed from training set and is regarded as verification set. On the basis of error evaluation indexes, the optimal parameter scheme of the model was selected. There were three indexes for model performance evaluation. Correlation coefficient (R), root mean square error (RMSE) and mean absolute error (MAE) (Eqs. (4)–(6)). R measures the similar degree of variation trend between $\text{PM}_{2.5}$ simulations and observations. Besides, RMSE and MAE estimate the bias between model outcomes and observations.

$$R = \frac{\sum_{i=1}^n (M_i - \bar{M})(O_i - \bar{O})}{\sqrt{\sum_{i=1}^n (M_i - \bar{M})^2(O_i - \bar{O})^2}} \quad (4)$$

$$\text{RMSE} = \sqrt{\frac{1}{n} \sum_{i=1}^n (O_i - M_i)^2} \quad (5)$$

$$\text{MAE} = \frac{\sum_{i=1}^n |O_i - M_i|}{n} \quad (6)$$

where n is the number of samples, $\text{PM}_{2.5}$ simulations and monitoring data are labeled as M_i and O_i , respectively. According to temporal-based CV results, the AC-RF model with optimal parameter was determined. At last, the monthly spatial dataset involving AOD, aerosol component AOD and meteorology factors during 1980–2020 were as AC-RF input. Monthly spatiotemporal datasets of $\text{PM}_{2.5}$ concentration with spatial resolution of 0.25° in recent 40 years was acquired.

2.3.3. $\text{PM}_{2.5}$ concentration spatiotemporal evolution analysis

The trend analysis of $\text{PM}_{2.5}$ pollution at pixel scale was calculated by Theil-Sen Median and Mann-Kendall methods in this research. Theil-Sen Median is a robust non-parametric statistical trend calculation method and less effected by outliers (Eqs. 7).

$$S_{PM_{2.5}} = \text{Median} \left(\frac{C_j - C_i}{j - i} \right) \quad (7)$$

where C_j and C_i refer to the annual concentration of $\text{PM}_{2.5}$ in j and i year, respectively. $1980 \leq i \leq j \leq 2020$. $S_{PM_{2.5}} > 0$ represents the increase trend of $\text{PM}_{2.5}$ variation. Otherwise, the decrease trend is reflected by $S_{PM_{2.5}} < 0$.

The significance of trend is estimated by Mann-Kendall method. It is usually combined with Theil-Sen Median method. Mann-Kendall method is a non-parametric statistical test and is competent for measuring the data obey any distribution (Eqs. 8–11).

$$S = \sum_{i=1}^{n-1} \sum_{j=n+1}^n \text{sgn}(C_j - C_i) \quad (8)$$

$$\text{sgn}(X_j - X_i) = \begin{cases} +1, & \text{if } (C_j - C_i) > 0 \\ 0, & \text{if } (C_j - C_i) = 0 \\ -1, & \text{if } (C_j - C_i) < 0 \end{cases} \quad (9)$$

$$\text{Var}(S) = \frac{n(n-1)(2n+5) - \sum_{p=1}^q t_p(t_p-1)(2t_p+5)}{18} \quad (10)$$

$$Z = \begin{cases} \frac{S-1}{\sqrt{\text{Var}(S)}}, & \text{if } S > 0 \\ 0, & \text{if } S = 0 \\ \frac{S+1}{\sqrt{\text{Var}(S)}}, & \text{if } S < 0 \end{cases} \quad (11)$$

where sgn refers to sign function. When $C_j - C_i > 0$, the value of $\text{sgn}(C_j - C_i)$ is 1. Otherwise, $C_j - C_i < 0$, $\text{sgn}(C_j - C_i) = -1$; $C_j - C_i = 0$, $\text{sgn}(C_j - C_i) = 0$. $\text{Var}(S)$ is variance of test statistics S . t_p and n are data series and the number of the p th group points, respectively. Z value is the basis for judging significance. When the absolute value of Z is larger than 1.96, the trend of $\text{PM}_{2.5}$ concentration is significant at 95% level. Besides, the combination of Theil-Sen Median and Mann-Kendall method has been widely applied for trend analysis in several relative research (Munir et al., 2013; Yin et al., 2021).

3. Result and discussion

3.1. AC-RF model verification

The results of sample-based CV, spatial-based CV and temporal-based CV for AC-RF model performance verification are shown in Fig. 3. AC-RF simulation is in good agreement with in-suit observations with R values of sample-based CV, spatial-based CV and temporal-based CV of 0.92, 0.90 and 0.86, respectively. Furthermore, RMSE and MAE results of these three CV methods all represent high accuracy with values of about $10 \mu\text{g}\cdot\text{m}^{-3}$. However, there is a phenomenon that AC-RF underestimated $\text{PM}_{2.5}$ concentration with the slope of fitting function of about 0.80, which reflects AC-RF underestimation for severe polluted situation. On the one hand, on the basis of RF algorithm principle, $\text{PM}_{2.5}$ simulation is the average value of CART decision outcomes that is the decision-making unit of AC-RF model. Thus, the maximum of $\text{PM}_{2.5}$ concentration is smoothed. Besides, the frequency of severe $\text{PM}_{2.5}$ episodes is low and easily overlooked. On the other hand, the model outcomes are based on the training dataset and extreme high concentration outside the range cannot be simulated (Requia et al., 2020). Thus, $\text{PM}_{2.5}$ concentration during extremely haze event is always underestimated. Besides, the $\text{PM}_{2.5}$ monitoring data obtained from US consulates in China, Taiwan Province and Hong Kong environmental protection administration was regarded as external testing dataset to validate the historical estimates. External validation exhibited poorer accuracy with R and RMSE values of 0.69 and $13.01 \mu\text{g}\cdot\text{m}^{-3}$. It may relate to the fact that these stations represent a centralized distribution in South China and the spatial heterogeneity is not significant. R value of external verification was lower than CV results and there was not large bias of RMSE values. Overall, AC-RF model is promising for capturing the monthly spatiotemporal characteristics of $\text{PM}_{2.5}$ across China. Besides, the comparison of AC-RF model and other statistical methods performance is showed in supplement material (Table S2).

3.2. The spatiotemporal characteristics of $\text{PM}_{2.5}$ concentration during 1980–2020

Based on spatiotemporal dataset of aerosol and meteorology factors, monthly $\text{PM}_{2.5}$ simulation during 1980–2020 with spatial resolution of 0.25° was acquired by using AC-RF model. Monthly $\text{PM}_{2.5}$ time series of two provincial capital cities of each region in China are showed in Fig. S1. Averaged by monthly $\text{PM}_{2.5}$ simulation, the time series of annual average $\text{PM}_{2.5}$ concentration in recent 40 years is shown in Fig. 4. Overall, there were 15 years in which $\text{PM}_{2.5}$ annual average concentration exceeded $35 \mu\text{g}\cdot\text{m}^{-3}$ of the secondary annual limits of national

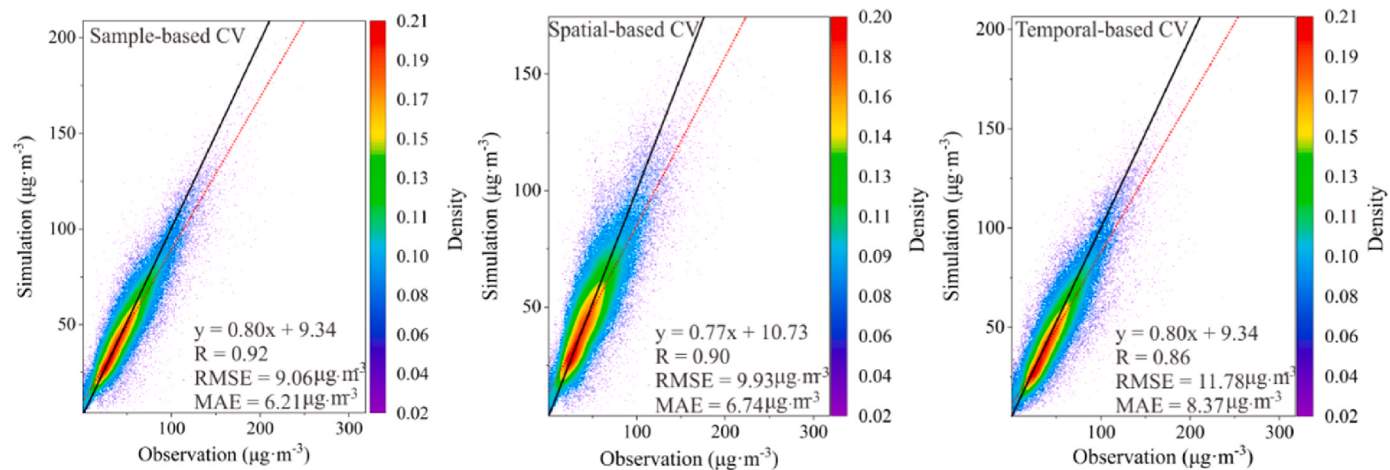


Fig. 3. CV results for AC-RF (The solid lines and red dashed lines represent linear regression line and 1:1 line, respectively). (For interpretation of the references to colour in this figure legend, the reader is referred to the Web version of this article.)

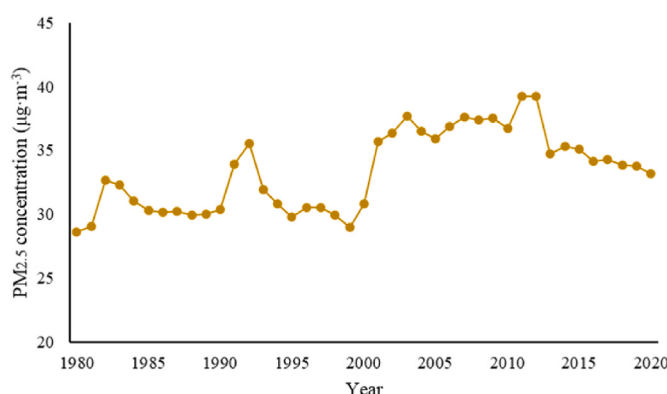


Fig. 4. The time series of annual PM_{2.5} concentration in China during 1980–2020.

ambient air quality standard (GB3095-2012). The turning points of PM_{2.5} annual concentration emerged in 1983, 1992, 2003 and 2012. The peak concentration of PM_{2.5} in 1983 and 1992 was closely correlated with the volcanic eruption of El Chichón in 1982 (Hay and Darby, 2010; Hirono and Shibata, 1983) and Pinatubo in 1992 (Skouratov, 1997). On the one hand, sharp increase of air pollutants results from large amount of volcanic ash and sulfide emitted by volcanic eruption. Besides, volcanic eruption events have a long-term effect on air quality. According to monitoring research in Vancouver, the maximum effect of El Chichón eruption on AOD was not felt until 9 months following the eruption and volcanic impact was still detectable even 18 months after the eruption (Hay and Darby, 2010). Strong influence of Pinatubo volcanic eruption on aerosols in Arctic was observed during 1993–1996 based on surface monitoring stations (Nagel et al., 1998). On the other hand, meteorology condition is influenced significantly by volcanic eruption events. The solar radiation absorbed by ash suspended in the air warms the upper atmosphere and caused stagnant atmosphere construction, which leads to the adverse impacts on pollutant diffusion (Fujiwara et al., 2015).

During the period from 2000 to 2012, PM_{2.5} concentration climbed at an accelerating rate and the annual average PM_{2.5} concentration of 47.23 μg·m⁻³ and exceeded 34.94% of national secondary standard. Since 2000, with fast development of power and heavy manufacturing serving as the largest contributor to PM_{2.5}, primary PM_{2.5} emissions and SO₂ dramatically increased (Guan et al., 2014; Qiao et al., 2018). The force of socioeconomic activities on atmospheric environment exceeded the carrying capacity of atmospheric environment gradually, which

gave rise to frequent outbreaks of haze episodes. During 2003, PM_{2.5} concentration reached the first peak. It was mainly related with OC aerosol increased in Northeast China (Fig. S3). Extensive open biomass burning caused large OC emission in 2003 (Lu et al., 2011). Although some air pollution control measures, like the installation of large-scale flue gas desulfurization in electricity plants, were implemented since 2005. SO₂ emissions reduced by 1.5 million tons and 17.5 million tons in 2005 and 2010, respectively (Zhang et al., 2012). This pollution control measure was limited and pollutants industrial processes and household sectors emission still increased progressively. PM_{2.5} emission increment during 2005–2014 correlated with the increase of PM_{2.5} from thermal power and building materials (Guan et al., 2014; Jin et al., 2017). Furthermore, because of the contribution of stable synoptic conditions in the context of global climate change, PM_{2.5} concentration climbed vertices in recent 40 years with the annual average concentration of 39.24 μg·m⁻³ across China in 2012 (Zhang et al., 2015).

Subsequently, the implementation of China Clean Air Act, the most stringent policies, improved air quality significantly in the context of the applied of various air pollutants emission reduction methods including production structure changes, clean energy adoption and the designation of new air quality criteria. According to estimation of Zheng et al. (2018), the emission of air pollutants including SO₂, NO_x, PM₁₀, PM_{2.5}, BC and OC all decreased by more than 20% after China clean air actions. Consequently, PM_{2.5} level declined gradually across China since 2013 (Silver et al., 2018; Li et al., 2019b). In 2020, PM_{2.5} concentration was the lowest of 33.17 μg·m⁻³ at national scale since 2015. Because of COVID-19 lockdown in China, anthropogenic source emission including road traffic, industry and power plants sharply decreased. Primary PM_{2.5} emission decreased by about 17% and PM_{2.5} components emission, such as BC and OC, reduction ratios are of 26% and 9% (Huang et al., 2021).

The spatiotemporal dynamic characteristics of PM_{2.5} concentration in China during 1980–2020 are described further in Fig. 5. From the spatial distribution of PM_{2.5} concentration perspective, there had been ever two severe polluted regions in China local in Xinjiang province and North China-Central China region. The high PM_{2.5} level in Xinjiang province is mainly influenced by underlying surface environment. Since the biggest desert called Taklimakan in central Xinjiang province is characterized as desert landscape and dry climate are the breeding ground for dust weather (Chen et al., 2017; Ma et al., 2020). Especially in spring, solar radiation enhancement leads to the increase of surface temperature and accelerates air movement (Balme and Greeley, 2006). Besides, the wind gap caused by topography and little ground friction resulted from limited precipitation and vegetation coverage are also the reasons for strong wind in these regions (Ma et al., 2020). Moreover, temperature increase caused sand source softening and dust entry into

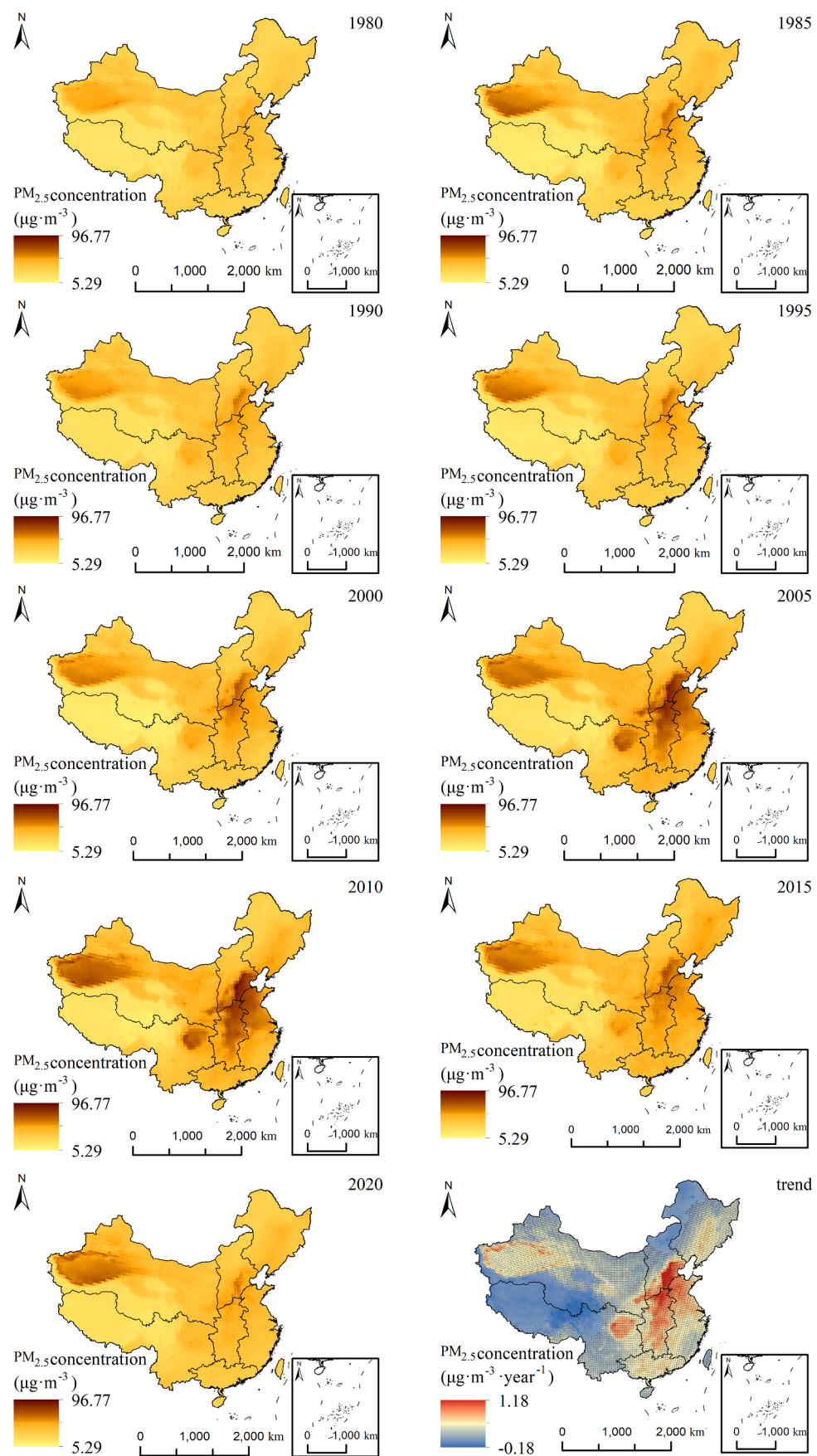


Fig. 5. The spatiotemporal distribution of annual $\text{PM}_{2.5}$ simulation in China during 1980–2020 (black dots signify the pass of significance test in trend analysis map).

air easily by means of upgrade air mass. Meanwhile, atmosphere transportation brings sand far from source area (Li et al., 2013). Thus, high level PM_{2.5} events were always accompanied by dust weather in Xinjiang province and even North China. According to PM_{2.5} concentration trend analysis, the rangeability of PM_{2.5} level in Xinjiang province was not distinct and the air quality in some regions was even improved. Benefit by the construction of northwest-north-northeast

China networks of shelterbelts, the frequency and intensity of sandstorms and PM_{2.5} pollution were improved in northern China to some extent in recent years (Zheng et al., 2019).

Since 1985, the air quality in Jing-Jin-Ji urban agglomeration, North China and Central China exacerbated gradually with the expansion of severe contaminated area. Overall, PM_{2.5} concentration in these regions exhibited significantly increase trend during study period. It is

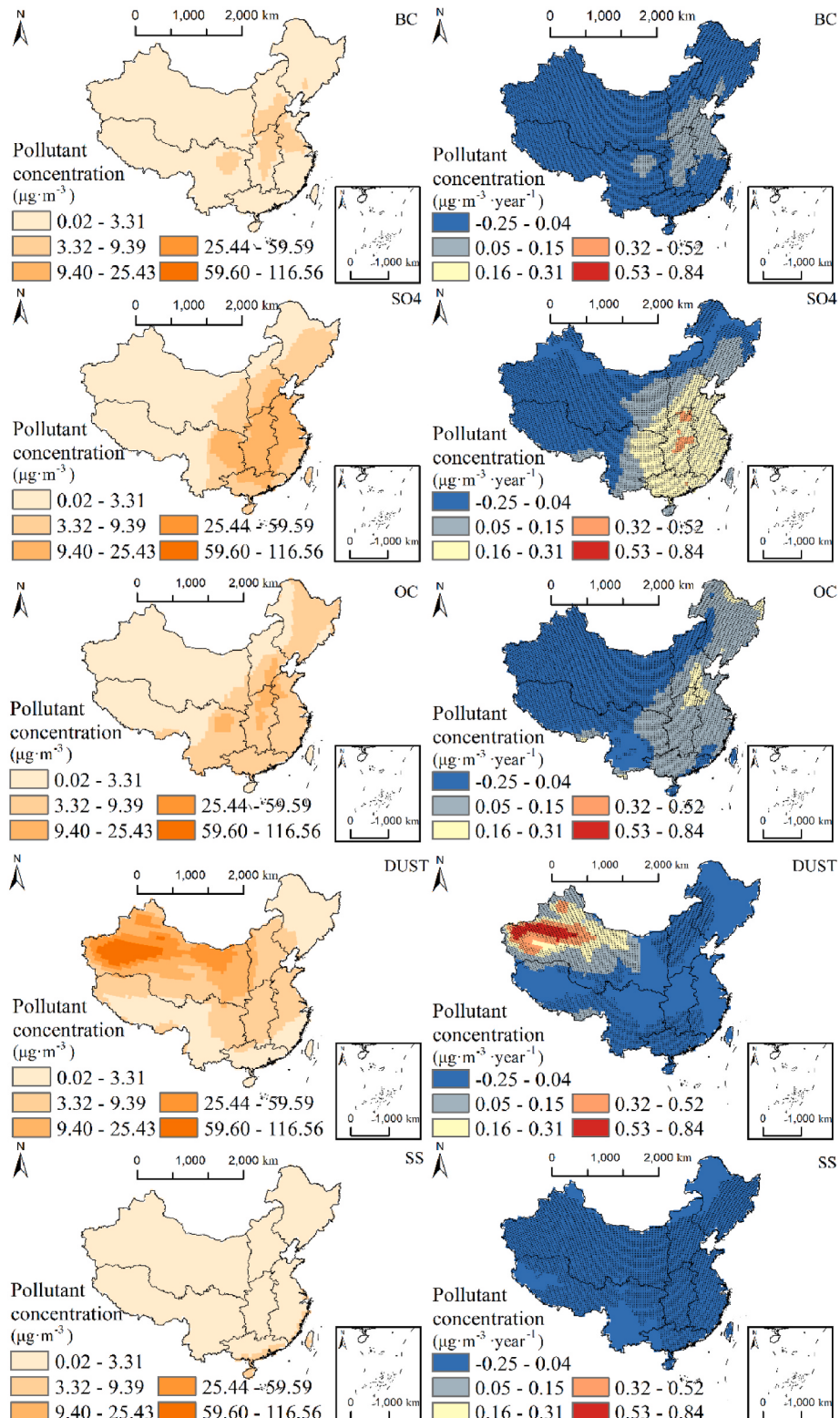


Fig. 6. Spatial distribution of 41-year average aerosol components concentration in China.

noticeable that population in these regions is accounted for about 27% of national population (Xu, 2017). The population exposure to high PM_{2.5} makes them face with high health threaten and economic losses are also rising. In contrast, air quality was in good grade in South China and Southwest China. Since warm and moist air flowing from the Pacific Ocean carries a lot of moisture to these regions. Frequent precipitation not only leads to high vegetation coverage which is not conducive to sand and dust weather formation, but also can wash suspended particles in atmosphere (Chen et al., 2018). In addition, cloudy weather results in the absorption of solar radiation and slows down secondary aerosol formation (Li et al., 2019a). In Southwest China especially the Tibet Plateau, atmosphere less affected by socioeconomic activities. Thus, anthropogenic air pollutants content in the atmosphere over Tibet Plateau is less than other regions. However, Sichuan basin in Southwest China also suffered from prominent haze weather. On the one hand, surrounded mountains reduce the wind speed in Sichuan basin, which prevents the dispersion of pollutants. On the other hand, Sichuan basin serves as population center and is the most active region in Southwest China. Anthropogenic emissions contribute much to the haze episodes in this region (Shi et al., 2020).

Subsequently, with the implementation of "Blue Sky Protection Campaign" and the most stringent policies to date, improvement in air quality has become more pronounced (Guan et al., 2014). Since 2015, PM_{2.5} concentration remarkably declined, especially in North China and Central China. The area of polluted regions also shrank. However, haze weather also emerged in some cities in North China, Northeast China, Central China and East China even during COVID-19 lock down with PM_{2.5} monthly concentration exceeded 100 $\mu\text{g}\cdot\text{m}^{-3}$ in January 2020 (Fig. S1). This PM_{2.5} pollution mainly caused by secondary PM_{2.5}, since NO_x emissions decrease from anthropogenic sources enhances atmospheric oxidizing capacity and results in the facilitation of secondary aerosol formation (Huang et al., 2021).

Based on the analysis above, severe natural disasters can cause the mutation of atmospheric pollutants concentration. However, the pressure force exerted by anthropogenic activities affects air quality at long term (Zhang et al., 2016). The influence of temporary human intervention on the change of atmospheric pollutants level is not significant. Besides, air pollution formation is extremely complex and control measures need to follow the principles of coordinated and balanced.

3.3. The spatiotemporal characteristics of aerosol components during 1980–2020

Based on MERRA-2 aerosol components dataset, the spatiotemporal evolutions of aerosol compositions concentration in China also have been investigated (Fig. 6, Fig. S2 and Fig. S3). SO₄ aerosol was the secondary major components in PM_{2.5} in China and represented the fastest growth rate except DUST aerosol. As for the distribution of aerosol species average level in these years, the spatial patterns of BC, SO₄ and OC aerosol were similar with high polluted area in southern North China, northern Central China and Sichuan basin. Since BC, OC and SO₄ are mainly emitted from the same sources and influenced by anthropogenic activities (Tian et al., 2016; Wang et al., 2016). The different was that SO₄ and OC aerosol concentration was also high in South China and East China. BC aerosol polluted area mainly distributed in southern North China, Central, northern East China and Sichuan province resulting from high BC emission and residential coal combustion (Wang et al., 2012). The severe air pollution in Taklimakan desert locating central Xinjiang province was polluted by DUST aerosol. Due to atmospheric transportation, the part of DUST aerosol in other region was also transported from vast desert in Northwest China (Zhang, 2015; Li et al., 2013). As for sea salt aerosol, it mainly comes from sea water droplets. Moreover, sea salt aerosol concentration is affected by the variation in sea surface height, sea wind and sea wave height (Liu et al., 2017). Consequently, sea salt aerosol concentration showed the distribution trend of decreasing concentration from coastal areas to inland

areas.

3.4. Influencing factors contributions to PM_{2.5} concentration

Node impurity average reduction of AC-RF model for PM_{2.5} retrieval can reflect the contribution of each factors to PM_{2.5} concentration (Fig. 7). It showed that BC exerted the most intensive impacts on PM_{2.5} concentration. On the basis of spatial correlation between aerosol components and PM_{2.5} (Fig. S3), evolution trend of BC and PM_{2.5} was consistent, especially in Central China, East China and South China with correlation coefficient of about 0.9. Besides, OC aerosol also had close positive correlation with PM_{2.5} variation in these regions during recent 40 years. As for the contribution of meteorology factors, T affected PM_{2.5} concentration variation by influencing atmospheric stability and photochemical reactions. In winter, stable synoptic conditions caused by inversion results in PM_{2.5} accumulation. In contrast, the increase of surface temperature accelerates atmospheric convection which is in favor of PM_{2.5} diffusion. It even brings precipitation and washes up suspended PM_{2.5}. Furthermore, T variation is also related with anthropogenic emission. Pollutant emission for household heating increases with T drop, especially in northern regions of China (Zhang et al., 2020). Consequently, PM_{2.5} concentration in China represented seasonal periodic variation with peak value emerging in winter and the cleanest air quality in summer (Fig. S1). Besides, SSRC and UVB also played essential roles in PM_{2.5} variation. According to spatial correlation between meteorology factors and PM_{2.5} concentration (Fig. S2), SSRC and UVB both negatively correlated with PM_{2.5} concentration in most regions of China. Since they are indexes reflecting solar radiation intensity and are closely related to variation of T. Although there was opposite variation trend between solar radiation and PM_{2.5} concentration from the long-term perspective, solar radiation intensity is of facilitation for secondary formation. Secondary PM_{2.5} formation is closely influenced by solar radiation intensity. With the economic rapid development, pollutant sources are gradually diversifying and secondary PM_{2.5} pollution become dominate. For example, secondary PM_{2.5} is of high percentage of 30%–77% in Beijing, Shanghai, Guangzhou and Xi'an during haze weather occurring in January 2013 (Huang et al., 2014). In particularly, UVB exerted positive influence on PM_{2.5} in Southwest China which had strong solar radiation (Fig. S2).

4. Conclusion

In order to fill the gap in the research about PM_{2.5} pattern

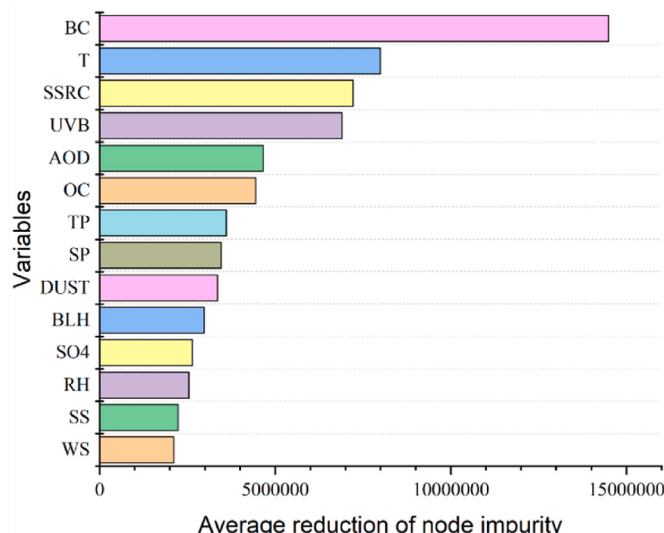


Fig. 7. Factors contributions to PM_{2.5} concentration.

heterogeneity from the perspective of components, a novel modeling scheme introducing aerosol species as explanatory variable for PM_{2.5} heterogenous formation mechanism was employed to reconstruct monthly PM_{2.5} concentration during 1980–2020. Furthermore, the spatiotemporal characteristics of aerosol components concentration were also detected to uncover PM_{2.5} evolution characteristics further. It indicated:

- 1) AC-RF model could be regarded as an efficient tool for reconstructing countrywide historical PM_{2.5} concentration. Three CVs methods, sample-based CV, spatial-based CV and temporal-based CV, results indicated worthy performance of AC-RF model with correlation coefficient (R) of 0.92, 0.90, 0.86, respectively.
- 2) Based on PM_{2.5} concentration retrieval dataset, spatiotemporal characteristics of PM_{2.5} was mapped and annual evolution characteristics of PM_{2.5} concentration could be approximately divided into three stages. Before 2000, the variation of PM_{2.5} concentration in China was mainly affected by natural factors. There were brief peaks of PM_{2.5} concentration in 1983 and 1992 influenced by the volcanic eruption of El Chichón and Pinatubo. Besides, the most polluted area located in Xinjiang province, North China, Central China. After 2000, PM_{2.5} concentration significantly increased with the prominent polluted center in Jing-Jin-Ji agglomeration and northern area of Central China. Industrial and socioeconomic activities are salient contribution to PM_{2.5} emission. With the implementation of a strictest-ever air pollution control policy, PM_{2.5} pollution in China substantially improved after 2012.
- 3) Aerosol components evolution in China also exhibited obviously spatiotemporal heterogeneity. Dust aerosol was preponderance species in PM_{2.5} in Northwest China and mainly derived from Taklimakan desert. While sulfate and black carbon aerosol concentrated in eastern region of China. Since the sharp increase in anthropogenic emission after 2000, sulfate aerosol concentration climbed dramatically and became the dominant component in PM_{2.5} in China. BC aerosol evolution was the most closely related to PM_{2.5} pollution. In Northeast China, OC aerosol surge was ascribed to extensive open biomass burning.
- 4) In light of the comprehensive analysis of PM_{2.5} spatiotemporal evolution, natural environment condition and socioeconomic development status during 1980–2020, the corollary is that natural and anthropogenic activities affect haze episodes in different degrees. On the one hand, severe natural disasters can induce the mutation of atmospheric pollutant concentration. Meanwhile, meteorology condition closest correlated with PM_{2.5} evolution. On the other hand, the influence of temporary human intervention on the change of atmospheric pollutant level is not significant. Consequently, the measures for controlling air pollution should be carried out strictly without interruption.

Credit author statement

Su Ding: Conceptualization, Investigation, Writing - Original Draft.
Zhiwei Wei: Writing -Review & Editing. **Jianhua He:** Writing - Review & Editing. **Dianfeng Liu:** Writing - Review & Editing. **Rong Zhao:** Writing -Review & Editing.

Declaration of competing interest

The authors declare that they have no known competing financial interests or personal relationships that could have appeared to influence the work reported in this paper.

Acknowledgements

This work was financially supported by Research Development Fund of Zhejiang A & F University (2020FR083), National Natural Science

Foundation of China (grant number: 41871301 and 41771429).

Appendix A. Supplementary data

Supplementary data to this article can be found online at <https://doi.org/10.1016/j.jenvman.2022.115983>.

References

- Balme, M., Greeley, R., 2006. Dust devils on earth and mars. *Rev. Geophys.* 44 (3).
- Bai, K., Ma, M., Chang, N.B., Gao, W., 2019. Spatiotemporal trend analysis for fine particulate matter concentrations in China using high-resolution satellite-derived and ground-measured PM2.5 data. *J. Environ. Manag.* 233, 530–542.
- Breiman, L., 2001. Random forests. *Mach. Learn.* 45 (1), 5–32.
- Buchard, V., Randes, C.A., da Silva, A.M., Darmenov, A., Colarco, P.R., Govindaraju, R., Ferrare, R., Hair, J., Beyersdorf, A.J., Ziembka, L.D., Yu, H., 2017. The MERRA-2 aerosol reanalysis, 1980 onward. Part II: evaluation and case studies. *J. Clim.* 30 (17), 6851–6872.
- Chameides, W.L., Yu, H., Liu, S.C., Bergin, M., Zhou, X., Mearns, L., Wang, G., Kiang, C. S., Saylor, R.D., Luo, C., Huang, Y., Steiner, A., Giorgi, F., 1999. Case study of the effects of atmospheric aerosols and regional haze on agriculture: an opportunity to enhance crop yields in China through emission controls? *Proc. Natl. Acad. Sci. U.S.A.* 96 (24), 13626–13633.
- Che, H.Z., Gui, K., Xia, X.G., Wang, Y.Q., Holben, B.N., Goloub, P., Cuevas-Agullo, E., Wang, H., Zheng, Y., Zhao, H.J., Zhang, X.Y., 2019. Large contribution of meteorological factors to inter-decadal changes in regional aerosol optical depth. *Atmos. Chem. Phys.* 19 (16), 10497–10523.
- Chen, S.Y., Huang, J.P., Kang, L.T., Wang, H., Ma, X.J., He, Y.L., Yuan, T.G., Yang, B., Huang, Z.W., Zhang, G.L., 2017. Emission, transport, and radiative effects of mineral dust from the Taklimakan and Gobi deserts: comparison of measurements and model results. *Atmos. Chem. Phys.* 17 (3), 2401–2421.
- Chen, Z.Y., Xie, X.M., Cai, J., Chen, D.J., Gao, B.B., He, B., Cheng, N.L., Xu, B., 2018. Understanding meteorological influences on PM2.5 concentrations across China: a temporal and spatial perspective. *Atmos. Chem. Phys.* 18 (8), 5343–5358.
- Ding, S., He, J.H., Liu, D.F., Zhang, R.T., Yu, S.Y., 2020. The spatially heterogeneous response of aerosol properties to anthropogenic activities and meteorology changes in China during 1980–2018 based on the singular value decomposition method. *Sci. Total Environ.* 724, 138135.
- Fujiwara, M., Hibino, T., Mehta, S.K., Gray, L., Mitchell, D., Anstey, J., 2015. Global temperature response to the major volcanic eruptions in multiple reanalysis data sets. *Atmos. Chem. Phys.* 15 (23), 13507–13518.
- Gao, M., Guttikunda, S.K., Carmichael, G.R., Wang, Y., Liu, Z., Stanier, C.O., Saide, P.E., Yu, M., 2015. Health impacts and economic losses assessment of the 2013 severe haze event in Beijing area. *Sci. Total Environ.* 511, 553–561.
- Global Modeling and Assimilation Office (GMAO), 2015. MERRA-2 tavgM_2d_aer_Nx: 2d, Monthly mean, Time-averaged, Single-Level, Assimilation, Aerosol Diagnostics V5, 12.4. Goddard Earth Sciences Data and Information Services Center (GES DISC), Greenbelt, MD, USA. Accessed: [Data Access Date], 10.5067/FH9A0MLJPC7N.
- Guan, D.B., Su, X., Zhang, Q., Peters, G.P., Liu, Z., Lei, Y., He, K.B., 2014. The socioeconomic drivers of China's primary PM2.5 emissions. *Environ. Res. Lett.* 9 (2).
- Guemard, C.A., Yang, D., 2020. Worldwide validation of CAMS and MERRA-2 reanalysis aerosol optical depth products using 15 years of AERONET observations. *Atmos. Environ.* 225, 117216.
- Hammer, M.S., van Donkelaar, A., Li, C., Lyapustin, A., Sayer, A.M., Hsu, N.C., Levy, R. C., Garay, M.J., Kalashnikova, O.V., Kahn, R.A., Brauer, M., Apte, J.S., Henze, D.K., Zhang, L., Zhang, Q., Ford, B., Pierce, J.R., Martin, R.V., 2020. Global estimates and long-term trends of fine particulate matter concentrations (1998–2018). *Environ. Sci. Technol.* 54 (13), 7879–7890.
- Hay, J.E., Darby, R., 2010. El Chichón – influence on aerosol optical depth and direct, diffuse and total solar irradiances at Vancouver, B.C. *Atmos.-Ocean* 22 (3), 354–368.
- He, Q., Huang, B., 2018a. Satellite-based high-resolution PM2.5 estimation over the Beijing-Tianjin-Hebei region of China using an improved geographically and temporally weighted regression model. *Environ. Pollut.* 236, 1027–1037.
- He, Q., Huang, B., 2018b. Satellite-based mapping of daily high-resolution ground PM 2.5 in China via space-time regression modeling. *Rem. Sens. Environ.* 206, 72–83.
- Hersbach, H., Bell, B., Berrisford, P., Hirahara, S., Horányi, A., Muñoz-Sabater, J., Nicolas, J., Peubey, C., Radu, R., Schepers, D., Simmons, A., Soci, C., Abdalla, S., Abellán, X., Balsamo, G., Bechtold, P., Biavati, G., Bidlot, J., Bonavita, M., De Chiara, G., Dahlgren, P., Dee, D., Diamantakis, M., Dragani, R., Flemming, J., Forbes, R., Fuentes, M., Geer, A., Haimberger, L., Healy, S., Hogan, R.J., Hölm, E., Janisková, M., Keeley, S., Laloyaux, P., Lopez, P., Lupu, C., Radnoti, G., de Rosnay, P., Rozum, I., Vamborg, F., Villaume, S., Thépaut, J.-N., 2020. The ERA5 global reanalysis. *Q. J. R. Meteorol. Soc.* 146 (730), 1999–2049.
- Hu, X., Waller, L.A., Lyapustin, A., Wang, Y., Al-Hamdan, M.Z., Crosson, W.L., Estes Jr., M.G., Estes, S.M., Quattrochi, D.A., Puttaswamy, S.J., Liu, Y., 2014. Estimating ground-level PM2.5 concentrations in the Southeastern United States using MAIAC AOD retrievals and a two-stage model. *Rem. Sens. Environ.* 140, 220–232.
- Huang, R., Zhang, Y., Bozzetti, C., Ho, K., Cao, J., Han, Y., Daellenbach, K.R., Slowik, J. G., Platt, S.M., Canonaco, F., Zotter, P., Wolf, R., Pieber, S.M., Bruns, E.A., Crippa, M., Ciarelli, G., Piazzalunga, A., Schwikowski, M., Abbaszade, G., Schnelle-Kreis, J., Zimmermann, R., An, Z., Szidat, S., Baltensperger, U., El Haddad, I.,

- Prevot, A.S.H., 2014. High secondary aerosol contribution to particulate pollution during haze events in China. *Nature* 514 (7521), 218–222.
- Hirono, M., Shibata, T., 1983. Enormous increase of stratospheric aerosols over Fukuoka due to volcanic eruption of El Chichon in 1982. *Geophys. Res. Lett.* 10 (2), 152–154.
- Huang, X., Ding, A., Gao, J., Zheng, B., Zhou, D., Qi, X., Tang, R., Wang, J., Ren, C., Nie, W., Chi, X., Xu, Z., Chen, L., Li, Y., Che, F., Pang, N., Wang, H., Tong, D., Qin, W., Cheng, W., Liu, W., Fu, Q., Liu, B., Chai, F., Davis, S.J., Zhang, Q., He, K., 2021. Enhanced secondary pollution offset reduction of primary emissions during COVID-19 lockdown in China. *Natl. Sci. Rev.* 8 (2), nwaa137.
- Hung, W., Lu, C., Wang, S., Chen, S., Tsai, F., Chou, C.C.K., 2019. Investigation of long-range transported PM2.5 events over Northern Taiwan during 2005–2015 winter seasons. *Atmos. Environ.* 217, 116920.
- Jin, Q., Fang, X., Wen, B., Shan, A., 2017. Spatio-temporal variations of PM2.5 emission in China from 2005 to 2014. *Chemosphere* 183, 429–436.
- Jiang, T., Chen, B., Nie, Z., Ren, Z., Xu, B., Tang, S., 2021. Estimation of hourly full-coverage PM2.5 concentrations at 1-km resolution in China using a two-stage random forest model. *Atmos. Res.* 248, 105146.
- Kishchka, P., da Silva, A., Starobinets, B., Long, C., Kalashnikova, O., Alpert, P., 2015. Saharan dust as a causal factor of hemispheric asymmetry in aerosols and cloud cover over the tropical Atlantic Ocean. *Int. J. Rem. Sens.* 36 (13), 3423–3445.
- Lelieveld, J., Evans, J.S., Fnais, M., Giannadaki, D., Pozzer, A., 2015. The contribution of outdoor air pollution sources to premature mortality on a global scale. *Nature* 525, 367–371.
- Li, H., Yang, Y., Wang, H., Li, B., Wang, P., Li, J., Liao, H., 2021. Constructing a spatiotemporally coherent long-term PM2.5 concentration dataset over China during 1980–2019 using a machine learning approach. *Sci. Total Environ.* 765, 144263.
- Li, K., Jacob, D.J., Liao, H., Shen, L., Zhang, Q., Bates, K.H., 2019a. Anthropogenic drivers of 2013–2017 trends in summer surface ozone in China. *Proc. Natl. Acad. Sci. U.S.A.* 116 (2), 422–427.
- Li, L., Li, J.J., Wang, R.B., Zheng, H.H., Shi, F., Ren, M., 2013. The analysis for the impact of dust-weather on the urban ambient air quality in China during 2005 ~ 2010. *Environmental Monitoring in China* 29 (3), 15–19.
- Li, R., Wang, Z., Cui, L., Fu, H., Zhang, L., Kong, L., Chen, W., Chen, J., 2019b. Air pollution characteristics in China during 2015–2016: spatiotemporal variations and key meteorological factors. *Sci. Total Environ.* 648, 902–915.
- Li, S., Chen, L., Huang, G., Lin, J., Yan, Y., Ni, R., Huo, Y., Wang, J., Liu, M., Weng, H., Wang, Y., Wang, Z., 2020. Retrieval of surface PM2.5 mass concentrations over north China using visibility measurements and GEOS-chem simulations. *Atmos. Environ.* 222.
- Liu, M., Bi, J., Ma, Z., 2017. Visibility-based PM2.5 concentrations in China: 1957–1964 and 1973–2014. *Environ. Sci. Technol.* 51 (22), 13161–13169.
- Li, Z.Q., Niu, F., Lee, K.H., Xin, J.Y., Hao, W.M., Nordgren, B., Wang, Y.S., Wang, P.C., 2007. Validation and understanding of moderate resolution imaging spectroradiometer aerosol products (C5) using ground-based measurements from the handheld Sun photometer network in China. *J. Geophys. Res. Atmos.* 112 (D22).
- Lim, S.S., Vos, T., Flaxman, A.D., Danaei, G., Shibuya, K., Adair-Rohani, H., AlMazroa, M. A., Amann, M., Anderson, H.R., Andrews, K.G., et al., 2013. A comparative risk assessment of burden of disease and injury attributable to 67 risk factors and risk factor clusters in 21 regions, 1990e2010: a systematic analysis for the global burden of disease study 2010. *Lancet* 380 (9859), 2224e2260.
- Liu, X.J., Xia, S.Y., Yang, Y., Wu, J.F., Zhou, Y.N., Ren, Y.W., 2020. Spatiotemporal dynamics and impacts of socioeconomic and natural conditions on PM2.5 in the Yangtze River Economic Belt. *Environ. Pollut.* 263 (Pt A), 114569.
- Lu, Z., Zhang, Q., Streets, D.G., 2011. Sulfur dioxide and primary carbonaceous aerosol emissions in China and India, 1996–2010. *Atmos. Chem. Phys.* 11 (18), 9839–9864.
- Ma, M., Yang, X., Zhou, C., He, Q., Mamtimin, A., 2020. Contributions of dusty weather and dust devil to dust emission amounts at the northern margin of the Taklimakan Desert. *Nat. Hazards* 103 (1), 1441–1454.
- Munir, S., Habeebulah, T.M., Seraji, A.R., Gabr, S.S., Mohammed, A.M.F., Morsy, E.A., 2013. Quantifying temporal trends of atmospheric pollutants in Makkah (1997–2012). *Atmos. Environ.* 77, 647–655.
- Nagel, D., Herber, A., Thomason, L.W., Leiterer, U., 1998. Vertical distribution of the spectral aerosol optical depth in the Arctic from 1993 to 1996. *J. Geophys. Res. Atmos.* 103 (D2), 1857–1870.
- Provencal, S., Buchard, V., da Silva, A.M., Leduc, R., Barrette, N., Elhacham, E., Wang, S. H., 2017. Evaluation of PM2.5 surface concentration simulated by version 1 of the NASA's MERRA aerosol reanalysis over Israel and Taiwan. *Aerosol Air Qual. Res.* 17 (1), 253–261.
- Qiao, X., Ying, Q., Li, X., Zhang, H., Hu, J., Tang, Y., Chen, X., 2018. Source apportionment of PM2.5 for 25 Chinese provincial capitals and municipalities using a source-oriented Community Multiscale Air Quality model. *Sci. Total Environ.* 612, 462–471.
- Randles, C.A., Da Silva, A.M., Buchard, V., Colarco, P.R., Darmenov, A., Govindaraju, R., Smirnov, A., Holben, B., Ferrare, R., Hair, J., Shinozuka, Y., Flynn, C.J., 2017. The MERRA-2 aerosol reanalysis, 1980 – onward, Part I: system description and data assimilation evaluation. *J. Clim.* 30 (17), 6823–6850.
- Rawat, P., Sarkar, S., Jia, S., Khillare, P.S., Sharma, B., 2019. Regional sulfate drives long-term rise in AOD over megacity Kolkata, India. *Atmos. Environ.* 209, 167–181.
- Requia, W.J., Di, Q., Silvern, R., Kelly, J.T., Koutrakis, P., Mickley, L.J., Sulprizio, M.P., Amini, H., Shi, L., Schwartz, J., 2020. An ensemble learning approach for estimating high spatiotemporal resolution of ground-level ozone in the contiguous United States. *Environ. Sci. Technol.* 54 (18), 11037–11047.
- Rizza, U., Mancinelli, E., Morichetti, M., Passerini, G., Virgili, S., 2019. Aerosol optical depth of the main aerosol species over Italian cities based on the NASA/MERRA-2 model reanalysis. *Atmosphere* 10 (11), 709.
- Shi, H.Q., Zeng, S.L., Li, H.N., 2020. Temporal and spatial distribution characteristics and influencing meteorological factors of air pollutants in Sichuan Basin. *Acta Sci. Circumstantiae* 40 (3), 763–778.
- Silver, B., Reddington, C.L., Arnold, S.R., Spracklen, D.V., 2018. Substantial changes in air pollution across China during 2015–2017. *Environ. Res. Lett.* 13 (11), 114012.
- Skouratov, S., 1997. Influence of the Pinatubo eruption on the aerosol optical depth in the Arctic in the summer of 1993. *Atmos. Res.* 44 (1–2), 125–132.
- Song, Z., Fu, D., Zhang, X., Wu, Y., Xia, X., He, J., Han, X., Zhang, R., Che, H., 2018. Diurnal and seasonal variability of PM2.5 and AOD in North China plain: comparison of MERRA-2 products and ground measurements. *Atmos. Environ.* 191, 70–78.
- Sun, E.W., Xu, X.F., Che, H.Z., Tang, Z.W., Gui, K., An, L.C., Lu, C.S., Shi, G.Y., 2019. Variation in MERRA-2 aerosol optical depth and absorption aerosol optical depth over China from 1980 to 2017. *J. Atmos. Sol. Terr. Phys.* 186, 8–19.
- Tai, A.P.K., Mickley, L.J., Jacob, D.J., 2010. Correlations between fine particulate matter (PM2.5) and meteorological variables in the United States: implications for the sensitivity of PM2.5 to climate change. *Atmos. Environ.* 44 (32), 3976–3984.
- Tian, S.L., Pan, Y.P., Wang, Y.S., 2016. Size-resolved source apportionment of particulate matter in urban Beijing during haze and non-haze episodes. *Atmos. Chem. Phys.* 16 (1), 1–19.
- van Donkelaar, A., Martin, R.V., Brauer, M., Kahn, R., Levy, R., Verdúzco, C., Villeneuve, P.J., 2010. Global estimates of ambient fine particulate matter concentrations from satellite-based aerosol optical depth: development and application. *Environ. Health Perspect.* 118 (6), 847–855.
- Wang, G., Zhang, R., Gomez, M.E., Yang, L., Zamora, M.L., Hu, M., Lin, Y., Peng, J., Guo, S., Meng, J., Li, J., Cheng, C., Hu, T., Ren, Y., Wang, Y., Gao, J., Cao, J., An, Z., Zhou, W., Li, G., Wang, J., Tian, P., Marrero-Ortiz, W., Secret, J., Du, Z., Zheng, J., Shang, D., Zeng, L., Shao, M., Wang, W., Huang, Y., Wang, Y., Zhu, Y., Li, Y., Hu, J., Pan, B., Cai, L., Cheng, Y., Ji, Y., Zhang, F., Rosenfeld, D., Liss, P.S., Duce, R.A., Kolb, C.E., Molina, M.J., 2016. Persistent sulfate formation from London Fog to Chinese haze. *Proc. Natl. Acad. Sci. U.S.A.* 113 (48), 13630–13635.
- Wang, R., Tao, S., Wang, W., Liu, J., Shen, H., Shen, G., Wang, B., Liu, X., Li, W., Huang, Y., Zhang, Y., Lu, Y., Chen, H., Chen, Y., Wang, C., Zhu, D., Wang, X., Li, B., Liu, W., Ma, J., 2012. Black carbon emissions in China from 1949 to 2050. *Environ. Sci. Technol.* 46 (14), 7595–7603.
- Wei, J., Li, Z., Lyapustin, A., Sun, L., Peng, Y., Xue, W., Su, T., Cribb, M., 2021. Reconstructing 1-km-resolution high-quality PM2.5 data records from 2000 to 2018 in China: spatiotemporal variations and policy implications. *Rem. Sens. Environ.* 252, 112136.
- Xu, X., 2017. China Population Spatial Distribution Kilometer Grid Data Set. Resource and Environmental Science Data Registration and Publishing System.
- Xu, X., Yang, X., Zhu, B., Tang, Z., Wu, H., Xie, L., 2020. Characteristics of MERRA-2 black carbon variation in east China during 2000–2016. *Atmos. Environ.* 222, 117140.
- Yin, S., Guo, M., Wang, X., Yamamoto, H., Ou, W., 2021. Spatiotemporal variation and distribution characteristics of crop residue burning in China from 2001 to 2018. *Environ. Pollut.* 268, 115849.
- Zhang, J., Liu, L., Xu, L., Lin, Q., Zhao, H., Wang, Z., Guo, S., Hu, M., Liu, D., Shi, Z., Huang, D., Li, W., 2020. Exploring wintertime regional haze in northeast China: role of coal and biomass burning. *Atmos. Chem. Phys.* 20 (9), 5355–5372.
- Zhang, Q., 2015. A heavy haze episode in Shanghai in December of 2013: characteristics, origins and implications. *Aerosol Air Qual. Res.* 15, 1881–1893.
- Zhang, Q., He, K.B., Huo, H., 2012. Cleaning China's air. *Nature* 484 (7393), 161–162.
- Zhang, X., Wu, Y., Gu, B., 2016. Characterization of haze episodes and factors contributing to their formation using a panel model. *Chemosphere* 149, 320–327.
- Zhang, X.Y., Wang, J.Z., Wang, Y.Q., Liu, H.L., Sun, J.Y., Zhang, Y.M., 2015. Changes in chemical components of aerosol particles in different haze regions in China from 2006 to 2013 and contribution of meteorological factors. *Atmos. Chem. Phys.* 15 (22), 12935–12952.
- Zhang, B., Tong, D., Li, M., Liu, F., Hong, C.P., Geng, G.N., Li, H.Y., Li, X., Peng, L.Q., Qi, J., Yan, L., Zhang, Y.X., Zhao, H.Y., Zheng, Y.X., He, K.B., Zhang, Q., 2018. Trends in China's anthropogenic emissions since 2010 as the consequence of clean air actions. *Atmos. Chem. Phys.* 18 (19), 14095–14111.
- Zheng, G.J., Duan, F.K., Su, H., Ma, Y.L., Cheng, Y., Zheng, B., Zhang, Q., Huang, T., Kimoto, T., Chang, D., Poschl, U., Cheng, Y.F., He, K.B., 2015. Exploring the severe winter haze in Beijing: the impact of synoptic weather, regional transport and heterogeneous reactions. *Atmos. Chem. Phys.* 15 (6), 2969–2983.
- Zheng, H., Zhao, B., Wang, S., Wang, T., Ding, D., Chang, X., Liu, K., Xing, J., Dong, Z., Aunan, K., Liu, T., Wu, X., Zhang, S., Wu, Y., 2019. Transition in source contributions of PM2.5 exposure and associated premature mortality in China during 2005–2015. *Environ. Int.* 132, 105111.